Synthesis and Characterization of Face-to-Face Arylsulfanyl and Phenoxyl Radicals Embedded in Mesoporous Silicas

Pierre Nabokoff, Guillaume Brulay, Cyrielle Dol, Guillaume Gerbaud, Bruno Guigliarelli, Emilien Etienne, Emily Bloch, Fabio Ziarelli, Eric Besson, Stéphane Gastaldi

Synthesis and Characterization of Face-to-Face Arylsulfanyl and Phenoxyl Radicals Embedded in Mesoporous Silicas.

Pierre Nabokoff,[a] Guillaume Brulay,[a] Cyrielle Dol,[a] Guillaume Gerbaud,*[b] Bruno Guigliarelli,[b] Emilien Etienne,[b] Emily Bloch,[c] Fabio Ziarelli,[d] Eric Besson,*[a] Stéphane Gastaldi *[a]

[a] Aix Marseille Univ, CNRS, ICR, Marseille, France.

[b] Aix Marseille Univ, CNRS, BIP, Marseille, France.

[c] Aix Marseille Univ, CNRS, MADIREL, Marseille, France.

[d] Aix Marseille Univ, CNRS, Centrale Marseille, FSCM, Marseille, France

E-mail : stephane.gastaldi@univ-amu.fr, eric.besson@univ-amu.fr, ggerbaud@imm.cnrs.fr

Table of Contents:

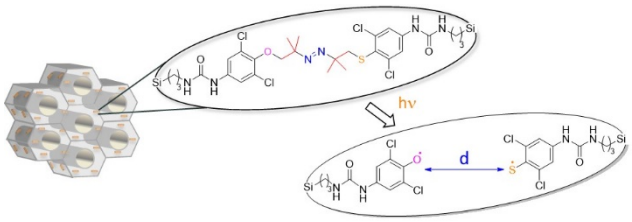

Abstract:

Recent applications of bi-, oligo- or polyradicals to spin sciences have generated considerable interest in the design of new bi/oligoradical organic molecules. Nevertheless, studies of physicochemical properties open shell systems are generally based on stable homonuclear organic radicals, which represent only a small portion of the existing radicals. In this context, diazene precursors of heteroatomic radicals were incorporated into the

SBA-15 silica framework. Photolysis at 360 nm of the diazene moiety resulted in the formation of two face-to-face oxygen- and sulfur-centered radicals. These systems were characterized by X-, Q- and W-band EPR spectroscopy by comparing them to silicas functionalized with either face-to-face sulfur-centered radicals or face-to-face oxygen-centered radicals. These EPR studies allowed measuring their half-life as well as their relaxation times (T_1 and T_2). The properties of silicas functionalized with sulfur-and oxygen-centered radicals fall between those measured for the two reference systems functionalized with only sulfur- or oxygen-centered radicals. These nanostructured silicas functionalized by two radicals of different nature are new potential candidates as polarizing agent for DNP NMR.

Introduction

Since the discovery of organic radicals, the reactivity of these elusive species has been deciphered and mastered providing a full range of invaluable transformations, which supplement nicely organic chemistry methodologies[1] as exemplified by the recent advances in photocatalysis.[2] These paramagnetic species also exhibit unique physico-chemical properties, which make them of the utmost importance in several domains. Indeed, the presence of unpaired electrons is the key structural feature leading to a wide array of applications such as energy storage,[3,4] activation of magnetic resonance contrast reagents,[5] spin probes for imaging and EPR spectroscopy,[6,7] opto-electronic,[8] molecular electronics[9,10] or polarizing agents for dynamic nuclear polarization (DNP).[11] Radicals implemented in these applications can be borne by simple molecules or incorporated into functional materials. Common points emerge from these systems: (i) the use of stable radicals[12] frequently based on trityl, verdazyl, or nitroxide radicals and (ii) the implementation of radicals of the same nature namely the recurrence/reiteration of an identical organic moiety.[13] Recent developments in the design of DNP polarizing agents

clearly show the interest of more sophisticated molecules involving the presence of two organic radicals of different nature. These agents take advantage of the features of two stable radicals, generally a 1,3-bisdiphenylene-2-phenylallyl (BDPA) or a trityl radical associated with a nitroxide radical, for improving the DNP NMR signal enhancement.[14,15,16,17,18,19] Up to now, it is necessary to recognize that no application, involving transient radicals and *a fortiori* two transient radicals of different nature, has been devised. The main reason is their high reactivity, which means short lifetimes for harvesting their physicochemical properties. This behaviour also explains the scarcity of materials or systems incorporating these elusive species. Consequently most of the radicals, namely the pool of transient radicals, continues to be unexplored for any application.

In earlier studies, we have shown that the lifetime of transient radicals, such as arylsulfanyl, arylsulfinyl or aryloxyl radicals could be amazingly improved when located in the frameworks[20,21,22] or on the pores[23,24] of nanostructured mesoporous silicas. The same trend was observed in polysilsesquioxane based lamellar materials or in periodic mesoporous organosilicas (PMOs).[22,25] These systems enabled to extend the lifetime of transient radicals from hundreds of microseconds to hours, days and even years, thanks to supramolecular interactions and to the absence of diffusion provided by the confinement which dramatically slowed down radical termination reactions.[26] These materials can be considered as platforms to study radical properties and, for instance, they afforded the measure of relaxation times of phenoxyl radical at low (50 K) and also at room temperature. Thus, longer electron relaxation times allow for greater signal enhancement in DNP NMR. These results clearly showed that it was possible to modulate the relaxation time by controlling the close surrounding of the radicals.[22]

The success of this strategy for the preparation of nanostructured materials functionalized with only one type of transient radical spurred us to tackle a more ambitious target: the

synthesis of mesoporous silicas functionalized with two face-to-face transient radicals of different nature. The purpose of these materials being to be used in an application, it was decided that the SBA-15 type silica met this objective for two reasons: (i) the use of the sol-gel process by direct synthesis in the presence of a surfactant allows the location and the homogeneous distribution of the organic molecules in the framework of the silica and (ii) the presence of mesopores which will facilitate the diffusion of molecules without direct interaction with the radicals embedded in the framework. In this article, we reported the synthesis of the radical precursor, its incorporation into the framework of a mesoporous silica through the sol-gel process and the EPR characterization of this multi-radical system.

Methods

Experimental procedures and characterization for the preparation of organic precursors and derived mesoporous silicas (NMR, nitrogen adsorption/desorption analysis, SAXS, ATG) are fully described in the supporting information.

Experimental Procedure for EPR analysis. X and Q-band EPR experiments were performed on a Bruker Elexsys E500 spectrometer with Q-band (ER5106 QT) or X-band SHQ high sensitivity (ER4122SHQE) Resonatorx and the Bruker BVT 3000 set-up or Oxford CF935 were used to control the temperature. W-band experiments were performed on a Bruker Elexsys E680 spectrometer equipped with a 6 T superconducting magnet and a 2-kG high-resolution sweep coil. Spectra were recorded with the standard W-band resonator fitted with a Bruker cryogen-free system (Stinger). The photolysis was directly performed in the cavity of the EPR spectrometer with a Hamamatsu LC8 01A light source with a 360-370 nm filter. For X-band EPR, the sample irradiation was performed before the introduction of the EPR tube in the cavity with a Rayonet apparatus (RPR-200, 16 UV lamps (360 nm)).

5 mg of fuctionalized silica were introduced in a 4 mm quartz-glass tube for X-band and in a 3 mm quartz-glass tube for Q and W-band, For experiments in the absence of oxygen, functionalized silicas were degassed with a 10^{-5} mbar vacuum pump and finally filled with argon. EPR spectra for direct observation of oxygen centered radical experiments were recorded with the parameters: X-band: modulation amplitude = 0.2 mT, receiver gain = 99 dB, modulation frequency = 100 kHz, power = 0.2 mW, sweep width = 20 mT, conversion time =

29.3 ms, sweep time = 30 s, number of scans = 2. Q-band: modulation amplitude = 0.1 mT, receiver gain = 50 dB, modulation frequency = 100 kHz, power = 0.1 mW, sweep width = 30 mT, conversion time = 81.9 ms, sweep time = 83.9 s, number of scans = 1. W-band: modulation amplitude = 0.3 mT, receiver gain = 26 dB, modulation frequency = 100 kHz, power = 0.005 mW, sweep width = 50 mT, conversion time = 81.9 ms, sweep time = 83.9 s, number of scans = 50.

Results and discussion

Material syntheses. The precursor design should meet several criteria: (i) be stable all along the silica preparation, (ii) generate cleanly and concomitantly upon the same conditions two radicals centered on different atoms and (iii) favour long radical lifetimes. Relying on previous results, arylsulfanyl[20] and aryloxyl[22] radicals were selected as model transient radical for this study. They can both be generated through a two-steps photochemically initiated process involving the decomposition of a diazene moiety and the β-fragmentation of the resulting tertiary carbon centered radical (Scheme 1).

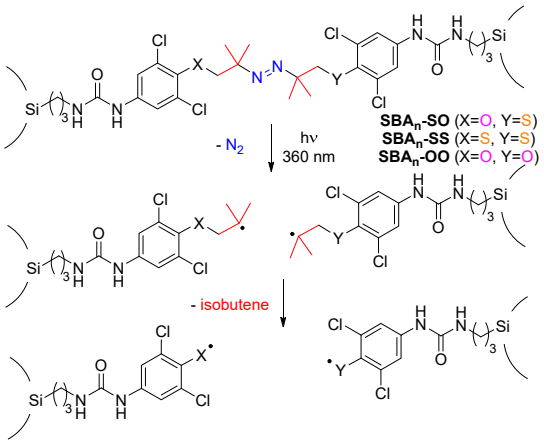

Scheme 1. Radical generation in the framework through diazene decomposition (**SBA$_n$-SO**, **SBA$_n$-SS** and **SBA$_n$-OO**)

It must underlined that the β-fragmentation reaction releasing the sulfur centered radical[27] occurred at least five order of magnitude faster than for the oxygen centered

radical ($k_f \approx 10^8$ s^{-1} versus $k_f < 10^3$ s^{-1}). However, at solid state, i.e. in the absence of the competitive pathway occurring in solution, this process enabled the clean generation of both radicals.[20,28] The presence of chlorine atoms in ortho positions of a phenoxyl radical prevents side reactions on these positions and, as a consequence, increases dramatically its lifetime.[22] It is the reason why all the ortho positions, with respect to the sulfur and the oxygen atoms, were protected with a chlorine atom. It must be pointed out that in this approach, all along the silica synthesis, the diazene moiety acts as a spacer between the oxygen and sulfur atoms. As consequence, once decomposed and because of the covalent anchoring of the organic precursor, both radicals cannot react together.

Reflecting all these considerations, SBA-15 type mesoporous silica was selected for this study. Throughout this article, the silicas were named SBAn-XY where SBA reminds the SBA-15 type structure and XY the nature of the atoms bearing the facing radicals (oxygen or sulfur). In order to substantiate the forthcoming EPR study of the multi-radical silicas generated from **SBA_n-SO**, analogous silicas **SBA_n-SS** and **SBA_n-OO**, functionalized with precursors of only sulfur- or only oxygen-centered radicals, were also prepared for having a characteristic signature of these radicals in these complex systems. **SBA_n-OO** was already available thanks to a previous investigation.[22] **SBA_n-SO** and **SBA_n-SS** were prepared from diazene **1** and **2** (Scheme 4). These precursors differ only by the nature of one atom, which was either an oxygen or a sulfur atom. They were both prepared from readily available diol **15**. The introduction of the two sulfur atoms was performed in a two steps sequence, formation of a triflate leaving group then substitution with potassium ethyl xanthogenate (Scheme 2). The deprotection of **17** led to dithiol **16** on which the correctly substituted aromatic rings were introduced through a nucleophilic aromatic substitution.

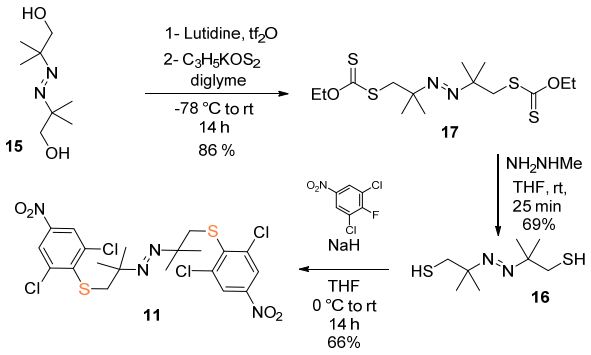

Scheme 2. Synthesis of diazene intermediate **11**

The synthetic approach of **1** was slightly different since a desymmetrisation of diol **15** was needed to introduce only one sulfur atom. The monoesterification of diol **15** was followed by the activation of the remaining alcohol and its substitution with potassium ethyl xanthogenate (Scheme 3). The simultaneous reduction of the ester group and the xanthate function on **13** with $AlLiH_4$ enabled the generation of the two targeted functions alcohol and thiol, which were used to insert the aromatic ring.

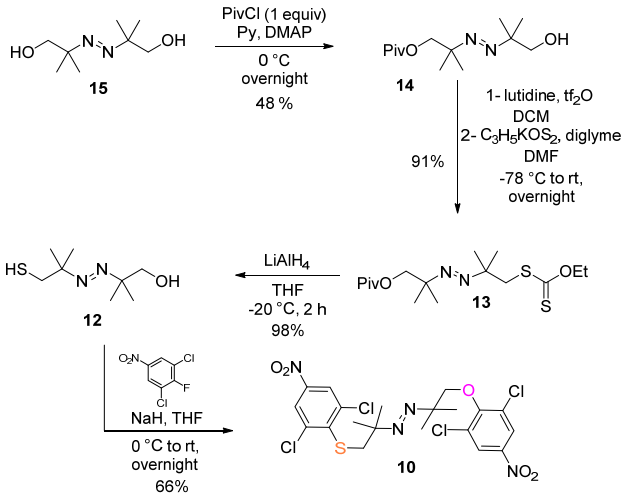

Scheme 3. Synthesis of diazene intermediate **10**

At this stage, the moiety for the generation of radicals was complete it remained to insert the linker for binding the precursor to the silica. The conversion of the advanced intermediates **10** and **11** into **1** and **2** needed the implementation of the same four steps: (i) the reduction of the nitro group into an amine, (ii) formation of the corresponding isocyanate, (iii) addition of allylamine to form the dissymmetric urea and (iv) the hydrosilylation of the double bond with

the triethoxysilane (Scheme 4). It could be underlined that the weak nucleophilic character of anilines **8** and **9** prevented their direct addition onto 3-(triethoxysilyl)propyl isocyanate. The triethoxysilyl groups were essential for the implementation of the sol-gel process.

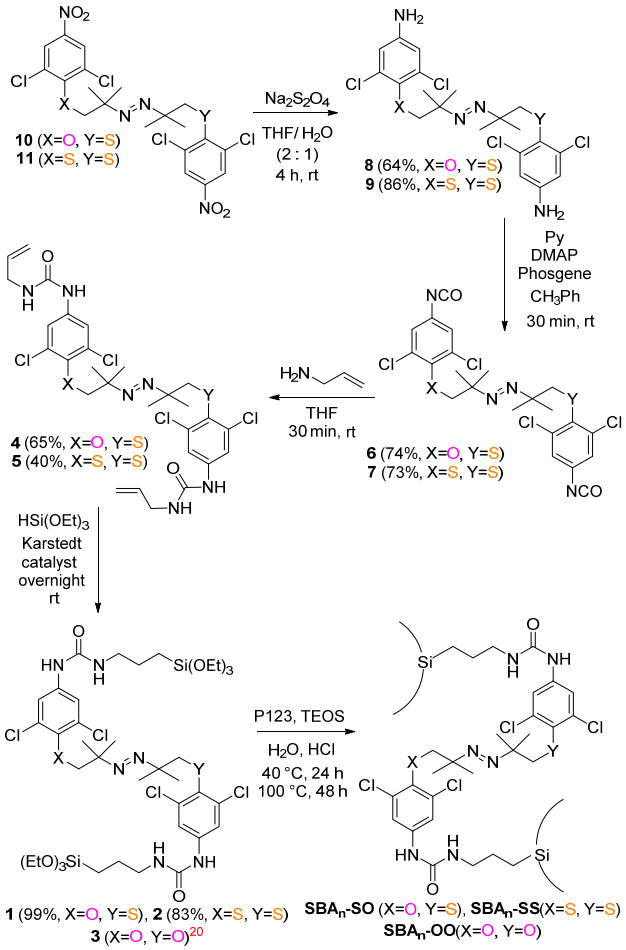

Scheme 4. Synthesis of SBA-15 mesoporous silicas **SBA$_n$-SO**, **SBA$_n$-SS** and **SBA$_n$-OO**

The functionalized 2D hexagonal SBA-15 type silicas were prepared by co-condensation of triethoxysilanes **1** or **2** with tetraethoxysilane (TEOS) in the presence of a structure directing agent (P123 ($PEO_{20}PPO_{70}PEO_{20}$)). The sol-gel process by direct synthesis is known to provide materials with a good level of nanostructuration and a homogeneous distribution of the organic silylated molecules in their walls.[29,30] The resulting materials were named **SBA$_n$-SO** in which **SO** specifies the nature of the radicals formed from this organic precursor and n indicates the TEOS/radical precursor molar ratio determined after the characterization of the hybrid silicas.

It should be noted that a decrease in the n value corresponds to an increase of the precursor concentration.

Thermogravimetry analysis (TGA) was used to find out the n value thanks to the peculiar loss of mass related to the diazene decomposition and the β-fragmentation between 130 and 220°C,[20] namely one molecule of dinitrogen and two molecules of isobutene (Figure 1). The overall mass loss corresponded to the quantity of precursors in the materials. Four and five different loadings were prepared for **SBA$_n$-SO** (n=38, 62, 110, 336) and **SBA$_n$-SS** (n= 36, 46, 217, 272, 570), respectively (see SI).

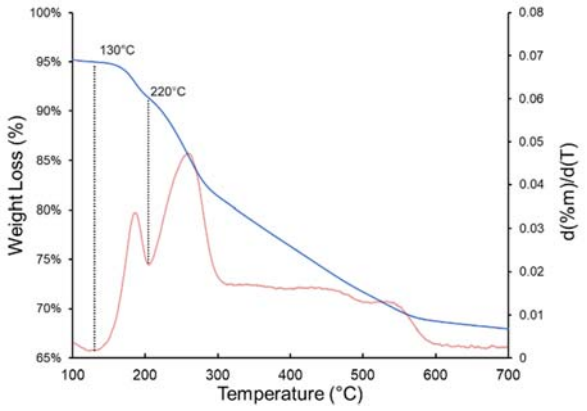

Figure 1. TGA of **SBA$_{36}$-SS**

All the materials were completely characterized by standard techniques (nitrogen adsorption/desorption analysis NMR, TGA, SAXS) (see SI). The main characteristics of these functionalized mesoporous silicas were collected in Table 1. The nitrogen adsorption–desorption isotherms of all materials measured at 77 K were type IV, with a H1-type hysteresis loop with high surface area (from 314 to 913 m^2/g) and pore size between 6.4 and 9.6 nm. According to the XRD patterns of the powders, functionalized silicas exhibited three well-resolved diffraction peaks which can be indexed as (100), (110) and (200) reflections, corresponding to a 2-D hexagonal structure. ^{13}C and ^{29}Si Cross Polarisation Magic Angle Spinning (CPMAS) NMR spectra of these silicas displayed (i) the integrity of the carbon skeleton of the radical precursors after the sol-gel process and

(ii) the presence of T^3 silicon (C-Si(O)$_3$) proving a covalent anchoring of the organic group onto the silicas thanks to a C-Si bond. It must be mentioned that in the case of low loadings, i.e. **SBA$_{336}$-SO** and **SBA$_{570}$-SS**, ^{13}C DNP SS NMR were performed to highlight the organic moieties (see SI).

Table 1. Physico-chemical characteristics of **SBA$_n$-SO** and **SBA$_n$-SS**

	[precursor][a] (µmol.g^{-1})	D_p (nm)	S_{BET} (m^2/g)	Vp (cm^3/g)	d_{100} (nm)	a_0 (nm)	Wall thickness (nm)
SBA$_{38}$-SO	563	9.6	314	0.9	11.6	13.4	3.8
SBA$_{62}$-SO	321	9.1	535	1.3	11.4	13.1	4.0
SBA$_{110}$-SO	227	7.8	593	1.4	10.7	12.3	4.5
SBA$_{336}$-SO	77	8.3	595	1.4	10.9	12.6	4.3
SBA$_{36}$-SS	436	7.6	554	1.2	11.9	13.7	6.1
SBA$_{46}$-SS	244	6.4	913	1.8	11.3	13.0	6.6
SBA$_{217}$-SS	121	7.6	589	1.0	10.9	12.6	5.0
SBA$_{272}$-SS	97	8.3	624	1.2	11.0	12.7	4.4
SBA$_{570}$-SS	48	8.3	690	1.3	10.9	12.7	4.4

[a] Concentration of **1** or **2** in the mesoporous silica determined with TGA.

EPR studies. The fragmentation of the radical precursor was triggered by direct irradiation of the silicas. The behaviour of radicals generated from **SBA$_n$-SO**, **SBA$_n$-SS** and **SBA$_n$-OO** was studied by EPR spectroscopy. The first series of experiments was performed directly in the cavity of an X band EPR spectrometer at 293K. The silica was irradiated in a 4 mm quartz-glass tube at 360 nm. Preliminary studies have shown that the presence of dioxygen did not impede EPR investigation of the phenoxyl radical incorporated into the wall of **SBAn-OO**. In order to evaluate the sensitivity of **SBA$_n$-SO** and **SBA$_n$-SS** towards dioxygen, kinetics of formation of radicals were performed under vacuum and air (Figure 2).[22]

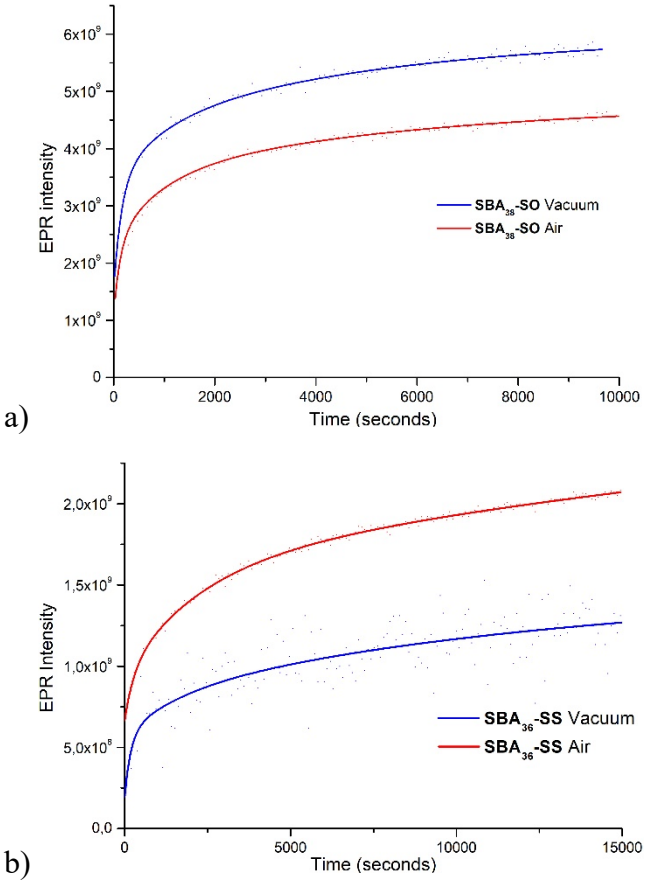

Figure 2. EPR growth curves of radicals generated from **SBA$_{38}$-SO** (a) and **SBA$_{36}$-SS** (b) under irradiation at 360 nm in the EPR cavity from the double integrated signal.

With both materials, these experiments clearly showed a moderate impact of dioxygen since the amount of radicals formed after 3h was nearly similar. These unexpected results may be analyzed through the reactivity of arylsulfanyl and aryloxyl radicals which are transient species in solution. In solution, the reaction of phenoxyl radicals with dioxygen is relatively slow[31] and does not compete with the fast dimerization reactions.[32] However, more stable 2,4,6-trisubstituted phenoxyl radicals can react with dioxygen.[33,34] When the 4-ureido-2,6-dichlorophenoxyl radical (Scheme 1) was covalently embedded in the framework of the silica, dimerization reactions were precluded because of the absence of diffusion whereas the coupling with dioxygen was still possible. The absence of dioxygen effect on the radical formation could be explained by a synergetic effect between the steric hindrance of the substituents on the aromatic ring and the wall of silica that can be perceived as an external radical protection. Concerning the sulfur centered radical in solution, dioxygen reacts rapidly[35,36] and reversibly[37]

with alkylsulfanyl radical to form thiyl peroxyl radicals which may evolve either through bimolecular processes or unimolecular rearrangement to sulfonyl radical.[38] However, arylsulfanyl radical behaves differently since its reversible coupling with dioxygen occurs five order of magnitude slower.[39] This low reactivity combined with, the absence of diffusion and the protection of the radical center by the ortho substituents and the silica wall contributed to the stability of the arylsulfanyl radical in SBA under air atmosphere. Under these conditions, half lifetimes of **SBA_{38}-SO** and **SBA_{36}-SS** were greater than 40 days.

According to these results, the following EPR studies were therefore performed under air.

To highlight the simultaneous formation of the arylsulfanyl and phenoxyl radicals in **SBA_n-SO**, silicas **SBA_n-SS** and **SBA_n-OO**, functionalized with precursors of only sulfur or only oxygen centered radicals, were first studied by EPR spectroscopy for having a characteristic signature of these radicals (Figure 3 a and b).

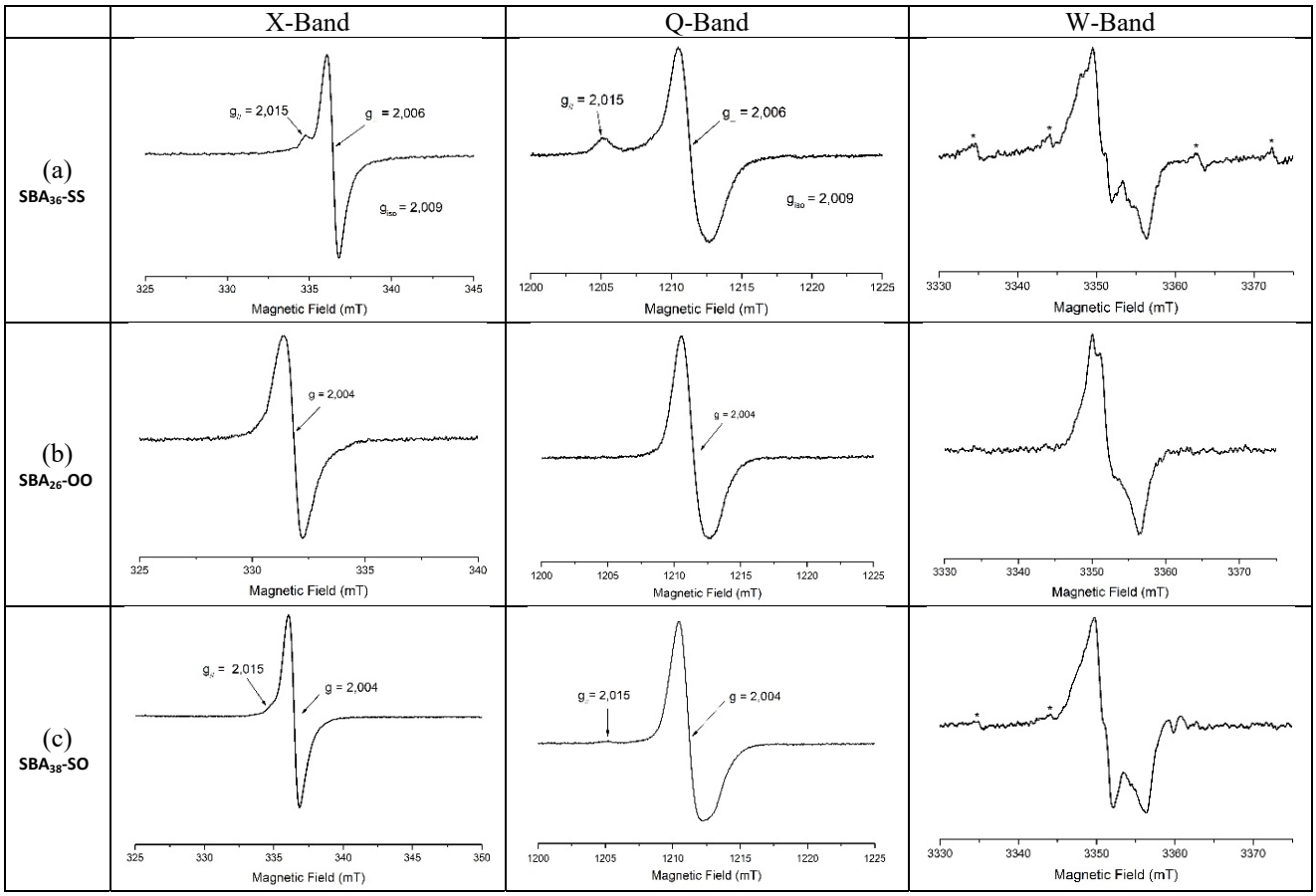

Figure 3. EPR spectra recorded at 9 (X band), 35 (Q band) and 95 (W band) GHz after irradiation of (a) **SBA$_{36}$-SS**, (b) **SBA$_{26}$-OO** and (c) **SBA$_{38}$-SO** (for experimental parameters, see SI).

CW-EPR X-band powder spectrum for **SBA$_n$-SS** showed a nearly axial anisotropic signal, resulting from the immobilization of the radicals characterized by $g_{//}$=2.015 and $g_{\perp}$ = 2.006, and a peak-to-peak line-width ΔHpp= 0.7 mT at X-band. These parameters are in agreement with the formation of arylsulfanyl radicals[40] for which the *g* tensor is axial and the spin density is localized on the sulfur atom. In the case of **SBA$_n$-OO**, an isotropic signal at *g* = 2.005 and a ΔHpp= 0.8 mT with an unresolved g-tensor anisotropy was recorded after irradiation. The Lande´ *g*-factors of this signal is in agreement with the formation of phenoxyl radicals.[41] The EPR studies of silicas functionalized with only sulfur- or oxygen centered- radicals have provided reference spectra for the characterization of **SBA$_n$-SO**.

SBA$_n$-SO was irradiated at 360 nm. The X-band powder spectrum (Figure 3c) exhibits mainly a broad and unresolved signal at *g* = 2.004 and and a ΔHpp= 0.8 mT. But the presence of a shoulder at the base of the main peak, at *g* = 2.015, is characteristic of the g parallel contribution observed for the arylsulfanyl radical. This signal at 2.015 is clearly an imprint of the presence of the arylsulfanyl radical. To increase the resolution, an investigation at higher frequency was performed. These experiments allowed a larger magnetic field range distribution of the *g*-tensors, often enabling the resolution of the **g**-tensor anisotropies, providing a molecular fingerprint for the organic radical assignment.

First Q-band CW-EPR spectra of **SBA$_{36}$-SS**, **SBA$_{19}$-OO** and **SBA$_{38}$-SO** were recorded at room temperature after irradiation at 360 nm. As expected for **SBA$_{36}$-SS,** i.e. S-centered radical, a better resolution was recorded for the g-tensor while for **SBA$_{19}$-OO**, i.e. O-centered radical, no anisotropy of the g tensor was revealed. In the case of **SBA$_{38}$-SO**, a shoulder on the negative component of the principal signal was observed as a better resolution of the g parallel component of the arylsulfanyl radical at *g* = 2.015. This observation and the line position at *g*

= 2.004 were consistent with the simultaneous presence of O- and S-centered radicals. This conclusion was ascertained with the W-band CW-EPR spectra of **SBA$_{36}$-SS**, **SBA$_{19}$-OO** and **SBA$_{38}$-SO** and enable to specify the g-values of the aryloxyl radical $g_{1,2,3}$ = 2.0071, 2.0059, 2.0035.

Electron spin relaxation properties of the radicals

These polyradical systems were then studied by pulsed EPR spectroscopy. Classical pulsed EPR experiments were recorded and analyzed as described in a previous paper in order to determine mean longitudinal relaxation times, $<T_{1e}>$, and spin-spin relaxation times, T_m, (Inversion-Recovery and spin-echo decay curves, respectively).[22] All the experiments were recorded at T=50K.

As with the Q-band CW-EPR study, the comparison of the X-band pulsed EPR field sweep showed the **SBA$_{38}$-SO** signal can be considered as a combinationof **SBA$_{36}$-SS** and **SBA$_{19}$-OO** signals. Indeed, the difference between **SBA$_{38}$-SO** (black line) and **SBA$_{36}$-SS** (red line) led to the blue line, which corresponded to the field sweep signal of **SBA$_{19}$-OO** (green line) (Figure 4).

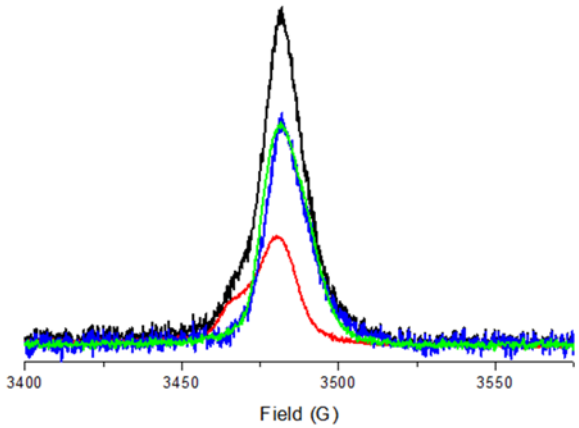

Figure 4. X-band pulsed EPR field sweep, Black line: **SBA$_{38}$-SO**. Red line: **SBA$_{36}$-SS**. Blue line: the difference between **SBA$_{38}$-SO** and **SBA$_{36}$-SS**. Green line: **SBA$_{19}$-OO**.

The mean longitudinal relaxation times were measured at the maximum of the absorption signal, $<T_{1e}>$ in Figure 5a, showed two significant trends. First, for all the **SBA_n-X** materials the $<T_{1e}>$ decreased as n increased, that is to say, when the radical concentration decreased. This behaviour was already observed in our previous study [22] and was attributed to the higher mobility of the radical at low loading in precursor. Second, the $<T_{1e}>$ increased in the series **SBA_n-SS**, **SBA_n-SO** and **SBA_n-OO** reflecting the influence of the spin-orbit contribution of the sulfur radical in the relaxation process. The more sulfur radicals were present the faster $<T_{1e}>$. This result was confirmed by the CW EPR saturation curves which exhibited the same behaviour (Figure 6).

The phase memory time, T_m in Figure 5b, followed the same behavior, with a longer T_m at high radical contents (small values of n) and when only oxygen radicals were involved. Nevertheless, no significant differences were observed between **SBA_n-SO** and **SBA_n-SS** for the T_m.

Thanks to the silica nanostructure, the relaxation time are longer than those measured in solution for the same radicals,[42] there are even longer than those of the nitroxides typically used in DNP NMR as polarizing agent.[43] In addition, two other points drew our attention: (i) **SBA_n-SO** exhibits relaxation times that are on the order of those of **SBA_n-OO** and (ii) the two sulfur- and oxygen-centered radicals have different *g*-values (see CW, X-, Q- and W-band results). These physicochemical properties make them potential candidates as polarizing agents for DNP SS NMR by implementing the Cross Effect mechanism,[11] which is one of the most efficient in DNP.

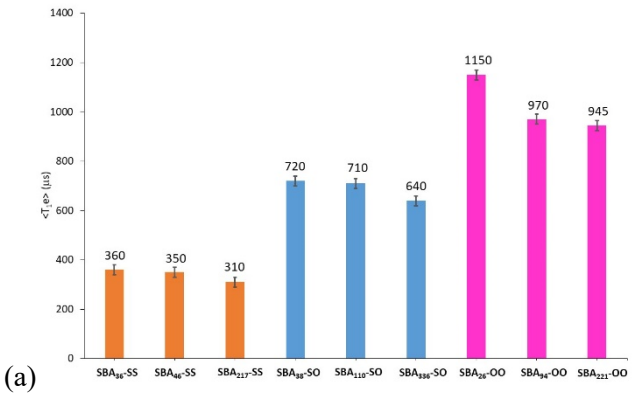

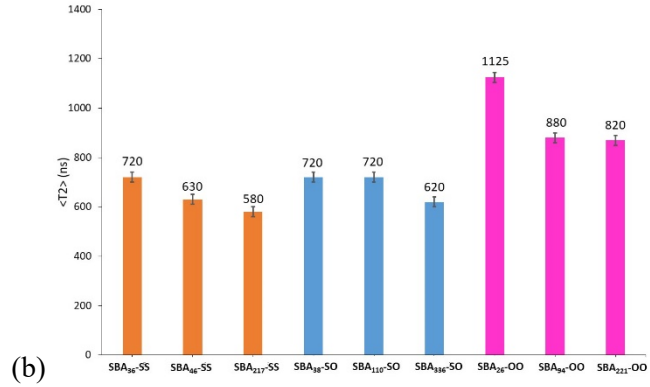

Figure 5. (a) Mean longitudinal relaxation time, $<T_{1e}>$, and (b) Phase memory time, T_m, as a function of the loading (precursor dilution) for **SBA$_n$-SO**, **SBA$_n$-SS** and **SBA$_n$-OO** materials at T=50K.

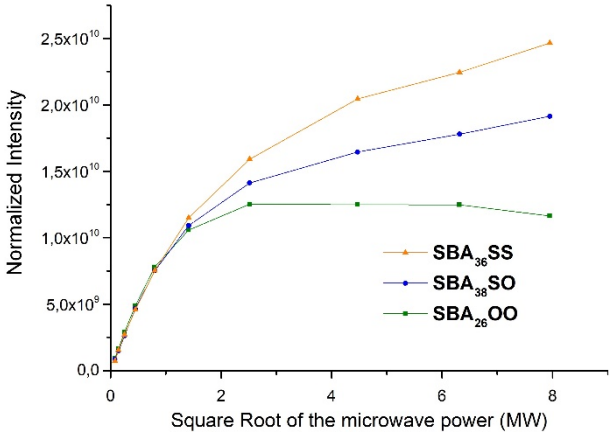

Figure 6. Saturation curves of **SBA$_{38}$-SO**, **SBA$_{36}$-SS** and **SBA$_{26}$-OO** at 293K from double integrated signal.

Conclusion

Increasing and controlling the complexity of new paramagnetic nanostructured materials is key to the development of new applications in spin sciences. In this study, it was demonstrated that it was possible to design and prepare nanostructured silicas in which two different transient radicals were positioned face-to-face. This was made possible by the flexibility of the sol-gel process which allowed the selective incorporation of an original radical precursor into the silica walls. The radicals were generated under mild irradiation conditions at room temperature. These polyradical silicas were characterized by EPR spectroscopy through comparison with reference silicas functionnalized with face-to-face oxygen-oxygen and sulfur-sulfur radicals. This study carried out with X-, Q- and W-band EPR spectrometers showed that these systems have physico-chemical properties between the two reference systems. In addition, these radicals have surprisingly long half-lives, making it possible to consider applications in areas where spin interaction is required.

ASSOCIATED CONTENT

Supporting Information: Characterizations for the organic compounds and the derived materials (NMR, SAXS, Nitrogen adsorption/desorption analysis, ATG). EPR growth and decay curves.

AUTHOR INFORMATION

Corresponding Author

*E-mail: stephane.gastaldi@univ-amu.fr, eric.besson@univ-amu.fr, ggerbaud@imm.cnrs.fr

Notes

The authors declare no competing financial interest.

ACKNOWLEDGMENTS : The authors acknowledge the Agence Nationale de la Recherche for funding (ANR-18-CE29-007). The authors are grateful to the EPRMRS facility of the

French Research Infrastructure INFRANALYTICS (FR2054) and the Aix-Marseille University EPR center.

References

[1] *Encyclopedia of Radicals in Chemistry, Biology and Materials*; Chatgilialoglu, C., Studer, A., Eds.; John Wiley & Sons Inc.: Chichester, Vol. 2, 2012.

[2] Buzzetti, L.; Crisenza, G. E. M.; Melchiorre P. Mechanistic Studies in Photocatalysis. *Angew. Chem. Int. Ed.* **2019**, *58*, 3730-3747.

[3] Friebe, C.; Schubert, U. S. High-Power-Density Organic Radical Batteries. *Top. Curr. Chem.* **2017**, *375*, 19.

[4] Wilcox, D. A.; Agarkar, V.; Mukherjee, S.; Boudouris, B. W. Stable Radical Materials for Energy Applications. *Annu. Rev. Chem. Biomol. Eng.* **2018**, *9*, 83-103.

[5] Nguyen, H. V.-T.; Chen, Q.; Paletta, J. T.; Harvey, P.; Jiang, Y.; Zhang, H.; Boska, M.D.; Ottaviani, M.F.; Jasanoff, A.; Rajca, A. et al. Nitroxide-Based Macromolecular Contrast Agents with Unprecedented Transverse Relaxivity and Stability for Magnetic Resonance Imaging of Tumors. *ACS Cent. Sci.* **2017**, *3*, 800-811.

[6] Haugland, M. M.; Lovett, J. E.; Anderson, E. A. Advances in the synthesis of nitroxide radicals for use in biomolecule spin labelling. *Chem. Soc. Rev.* **2018**, *47*, 668-680.

[7] Pierro, A.; Bonucci, A.; Normanno, D.; Ansaldi, M.; Pilet, E.; Ouari, O.; Guigliarelli, B.; Etienne, E.; Gerbaud, G.; Magalon, A. et al. Probing Structural Dynamics of a Bacterial Chaperone in Its Native Environment by Nitroxide-Based EPR Spectroscopy. *Chem. Eur. J.* **2022**, *28*, e202202249.

[8] Ratera, I.; Veciana J. Playing with organic radicals as building blocks for functional molecularmaterials. *Chem. Soc. Rev*. **2012**, *41*, 303-349.

[9] Sugawara, T.; Komatsu, H.; Suzuki, K. Interplay between magnetism and conductivity derived from spin-polarized donor radicals. *Chem. Soc. Rev.* **2011**, *40*, 3105-3118.

[10] Sanvito, S. Molecular Spintronic. *Chem. Soc. Rev.* **2011**, *40*, 3336-3355.

[11] Ni, Q. Z. ; Daviso, E.; Can, T. V.; Markhasin, E.; Jawla, S. K.; Swager, T. M.; Temkin, R. J.; Herzfeld, J.; Griffin, R. G. High Frequency Dynamic Nuclear Polarization. *Acc. Chem. Res.* **2013**, *46*, 1933-1941.

[12] Griller, D.; Ingold, K. U. Persistent Carbon-Centered radicals. *Acc. Chem. Res.* **1976**, *9*, 13-19.

[13] Oyaizu, K. ; Nishide, H. In *Encyclopedia of Radicals in Chemistry, Biology and Materials*; Chatgilialoglu, C., Studer, A., Eds.; John Wiley & Sons Inc.: Chichester, 2012,Vol. 4, pp 2163-2170.

[14] Dane, E. L.; Maly, T.; Debelouchina, G. T.; Griffin, R. G.; Swager, T. M. Synthesis of a BDPA-TEMPO Biradical. *Org. Lett.* **2009**, *11*, 1871-1874.

[15] Mathies, G.; Caporini, M. A.; Michaelis, V. K.; Liu, Y.; Hu, K.-N.; Mance, D.; Zweier, J. L.; Rosay, M.; Baldus, M.; Griffin, R. G. Efficient Dynamic Nuclear Polarization at 800 MHz/527 GHz with Trityl-Nitroxide Biradicals. *Angew. Chem. Int. Ed.* **2015**, *54*, 11770-11774.

[16] Liu, Y.; Villamena, F. A.; Rockenbauer, A.; Song, Y.; Zweier, J. L. Structural Factors Controlling the Spin−Spin Exchange Coupling : EPR Spectroscopic Studies of Highly Asymmetric Trityl−Nitroxide Biradicals. *J. Am. Chem. Soc.* **2013**, *135*, 2350-2356.

[17] Zhai, W.; Feng, Y.; Liu, H.; Rockenbauer, A.; Mance, D.; Li, S.; Song, Y.; Baldus, M.; Liu, Y. Diastereoisomers of l-proline-linked trityl-nitroxide biradicals: synthesis and effect of chiral configurations on exchange interactions. *Chem. Sci.* **2018**, *9*, 4381-4391.

[18] Wisser, D.; Karthikeyan, G.; Lund, A.; Casano, G.; Karoui, H.; Yulikov, M.; Menzildjian, G.; Pinon, A. C.; Purea, A.; Engelke, F. et al. BDPA-Nitroxide Biradicals Tailored for Efficient Dynamic Nuclear Polarization Enhanced Solid-State NMR at Magnetic Fields up to 21.1 T. *J. Am. Chem. Soc.* **2018**, *140*, 13340-13349.

[19] Berruyer, P.; Björgvinsdóttir, S.; Bertarello, A.; Stevanato, G.; Rao, Y.; Karthikeyan, G.; Casano, G.; Ouari, O.; Lelli, M.; Reiter, C. et al. Dynamic Nuclear Polarization Enhancement of 200 at 21.15 T Enabled by 65 kHz Magic Angle Spinning. *J. Phys. Chem. Lett.* **2020**, *11*, 8386−8391.

[20] Vibert, F.; Marque, S. R. A.; Bloch, E.; Queyroy, S.; Bertrand, M. P.; Gastaldi, S.; Besson, E. Design of Wall-Functionalized Hybrid Silicas Containing Diazene Radical Precursors. EPR Investigation of their Photolysis and Thermolysis. *J. Phys. Chem. C.* **2015**, *119*, 5434-5439.

[21] Vibert, F.; Bloch, E.; Bertrand, M. P.; Gastaldi, S.; Besson, E. Nanostructured Silicas, a Platform for the Observation of Transient Radicals: Application to Sulfinyl Radicals. *J. Phys. Chem. C.* **2018**, *122*, 681-686.

[22] Dol, C.; Gerbaud, G.; Guigliarelli, B.; Bloch, E.; Gastaldi, S.; Besson, E. Modulating lifetimes and relaxation times of phenoxyl radicals through their incorporation into different hybrid nanostructures. *Phys. Chem. Chem Phys.* **2019**, *21*, 16337-16344.

[23] Vibert, F.; Marque, S. R. A.; Bloch, E.; Queyroy, S.; Bertrand, M. P.; Gastaldi, S.; Besson, E. Arylsulfanyl Radical Lifetime in Nanostructured Silica: Dramatic Effect of the Organic Monolayer Structure. *Chem. Sci.* **2014**, *5*, 4716-4723.

[24] Vibert, F.; Bloch, E.; Bertrand, M. P.; Queyroy, S.; Gastaldi, S.; Besson E. Evidence for the Contribution of Degenerate Hydrogen Atom Transport to the Persistence of Sulfanyl Radicals Anchored to Nanostructured Hybrid Materials. *New J. Chem.* **2017**, *41*, 6678-6684.

[25] Dol, C.; Vibert, F.; Bertrand, M. P.; Lalevée, J.; Gastaldi, S.; Besson E. Diazene-Functionalized Lamellar Materials as Nanobuilding Blocks: Application as Light Sensitive Fillers to Initiate Radical PhotoPolymerizations. *ACS Macro Lett.* **2017**, *6*, 117-120.

[26] Bertrand, M. P.; Besson, E.; Gastaldi, S. In *Science of Synthesis: Free Radicals: Fundamentals and Applications in Organic Synthesis*, Fensterbank, L.; Ollivier, C., Eds.; Thieme: Stuttgart, 2021; Vol. 1, pp 5-28.

[27] Chatgilialoglu C.; Altieri, A.; Fischer, H. The Kinetics of Thiyl Radical-Induced Reactions of Monounsaturated Fatty Acid Esters. *J. Am. Chem. Soc.* **2002**, *124*, 12816-12823.

[28] Dol, C.; Bertrand, M. P.; Gastaldi, S.; Besson, E. Solid State Generation of Phenoxyl Radicals through β-Fragmentation from Specifically Designed Diazenes. An ESR Investigation. *Tetrahedron* **2016**, *72*, 7744-7748.

[29] Mehdi, A.; Reye, C.; Corriu, R. From molecular chemistry to hybrid nanomaterials. Design and functionalization. *Chem. Soc. Rev.* **2011**, *40*, 563-574.

[30] Lofgreen, J. E.; Ozin, G. A. Controlling morphology and porosity to improve performance of molecularly imprinted sol-gel silica. *Chem. Soc. Rev.* **2014**, *43*, 911-933.

[31] Maillard, B.; Ingold, K. U.; Scaiano, J. C. Rate Constants for the Reactions of Free Radicals with Oxygen in Solution. *J. Am. Chem. Soc.* **1983**, *105*, 5095-5099.

[32] Steenken, S.; Neta, P. In *The chemistry of phenols*. Rappoport, Z., Eds.; Wiley, 2003; Part 1, pp 1107-1152.

[33] Horswill, E. C.; Ingold, K. U. The Oxidation of Phenols. The Oxidation of 2,4-di-t-Butylphenol with Peroxy Radicals. *Can. J. Chem*. **1966**, *44*, 269-277.

[34] Griva, A. P.; Denisov, E. T. Kinetics of the Reactions of 2,4,6-Tri-t-butylphenoxyl with Cumene Hydroperoxide, Cumylperoxyl Radicals, and Molecular Oxygen. *Int. J. Chem. Kinet.* **1973**, *5*, 869-877.

[35] Schäfer, K.; Bonifacic, M.; Bahnemann, D.; Asmus, K.-D. Addition of Oxygen to Organic Sulfur Radicals. *J. Phys. Chem.* **1978**, *82*, 2777-2780.

[36] Mönig, J.; Asmus, K.-D.; Forni, L. G.; Willson, R. L. On the reaction of molecular oxygen with thiyl radicals : a re-examination *Int. J. Radiat. Biol* . **1987**, *52*, 589-602.

[37] Turnipseed, A. A.; Barone, S. B.; Ravishankara, A. R. Observation of CH_3S Addltion to O_2 in the Gas Phase. *J. Phys. Chem.* **1992**, *96*, 7502-7505.

[38] Razskazovskii, Y.; Colson, A.-O.; Sevilla, M. D. Nature of the Thiyl Peroxyl Radical: ESR and ab Initio MO Evidence for Intermolecular Stabilization of the Charge Transfer State, $RS^{+}SOO^{\bullet -}$. *J. Phys. Chem*. **1995**, *99*, 7993-8001.

[39] Ito, O.; Matsuda, M. Evaluation of Addition Rates of p-Chlorobenzenethiyl Radical to Vinyl Monomers by Means of Flash Photolysis. *J. Am. Chem. Soc.* **1979**, *101*, 1815-1819.

[40] Mörke, W.; Jezierski, A.; Singer, H. Nachweis von Arylschwefelradikalen mittels EPR. *Z. Chem*. **1979**, *19*, 147-148.

[41] Kaneko, T; Iwamura, K.; Nishikawa, R.; Teraguchi, M.; Aoki, T. Synthesis of sequential poly(1,3-phenyleneethynylene)-based polyradicals and through-space antiferromagnetic interaction of their solid state *Polymer* **2014**, 55, 1097-1102.

[42] Yamauchi, J.; Yamaji, T.; Katayama, A. Spin-lattice and spin-spin relaxation times of 2,4,6-tri-tert-butyl phenoxyl and 2,6-di-tert-butyl-4-methyl phenoxyl in diamagnetic crystals: Relaxation mechanism and influence of molecular motions. *Appl. Magn. Reson*. **2003**, *25*, 209-216.

[43] Kubicki, D. J.; Casano, G.; Schwarzwälder, M.; Abel, S.; Sauvée, C.; Ganesan, K.; Yulikov, M.; Rossini, A. J.; Jeschke, G.; Copéret, C. et al. Rational design of dinitroxide biradicals for efficient cross-effect dynamic nuclear polarization. *Chem. Sci.* **2016**, *7*, 550-558.